Available online at www.sciencedirect.com
ScienceDirect
C. R. Physique 9 (2008) 595–607
COMPTES RENDUS PHYSIQUE
http://france.elsevier.com/direct/COMREN/

Synchrotron x-rays and condensed matter / Rayonnement X synchrotron et matière condensée

Nuclear resonance scattering

Rudolf Rüffer

European Synchrotron Radiation Facility (ESRF), BP 220, 6, rue Jules-Horowitz, 38043 Grenoble cedex, France

Available online 23 October 2007

Abstract

Nuclear resonance scattering is an atomistic spectroscopy sensitive to magnetic and electronic properties as well as slow and fast structural dynamics. Applications, which take advantage of both the outstanding properties of third generation synchrotron radiation sources and those of the Mössbauer effect, benefit most. Examples resulting from investigations at the ESRF will be given in applications to high pressure and low temperatures, nano-scale materials, and dynamics of disordered systems. ***To cite this article: R. Rüffer, C. R. Physique 9 (2008).***

Résumé

La diffusion nucléaire résonnante. La diffusion nucléaire résonnante est une spectroscopie atomique sensible aux propriétés magnétiques et électroniques mais aussi aux dynamiques structurales lente et rapide. Elle prend tout son intérêt dans les applications qui tirent avantage des propriétés remarquables des sources de radiation synchrotron de troisième génération et de l'effet Mössbauer. Nous donnerons des exemples tirés de recherches menées à l'ESRF dans les domaines des hautes pressions et des basses températures, des nano-matériaux et de la dynamique des sytèmes désordonnés. ***Pour citer cet article : R. Rüffer, C. R. Physique 9 (2008).***

Keywords: Nuclear resonance scattering; Hyperfine interaction; Structural dynamics

Mots-clés : Diffusion nucléaire résonnante ; Interaction hyperfine ; Dynamiques structurales

1. Introduction

Nuclear resonance scattering rapidly developed with the advent of third generation synchrotron radiation sources to a versatile spectroscopy covering the fields of 'hyperfine spectroscopy' and 'structural dynamics'. In hyperfine spectroscopy it yields information on atomic, magnetic and electric properties and structures. Those fields of applications benefit most which exploit the specific properties of synchrotron radiation: applications to high pressure, to surfaces and multilayer structures, to single crystals, and to very small samples. Structural dynamics on a ps to μs timescale as free or jump diffusion as well as rotational motions can directly be measured in the time domain by nuclear quasi-elastic scattering techniques. On the fast timescale the (partial) vibrational density of states is directly accessible by nuclear inelastic scattering.

E-mail address: rueffer@esrf.fr.

1631-0705/$ – see front matter
doi:10.1016/j.crhy.2007.06.003

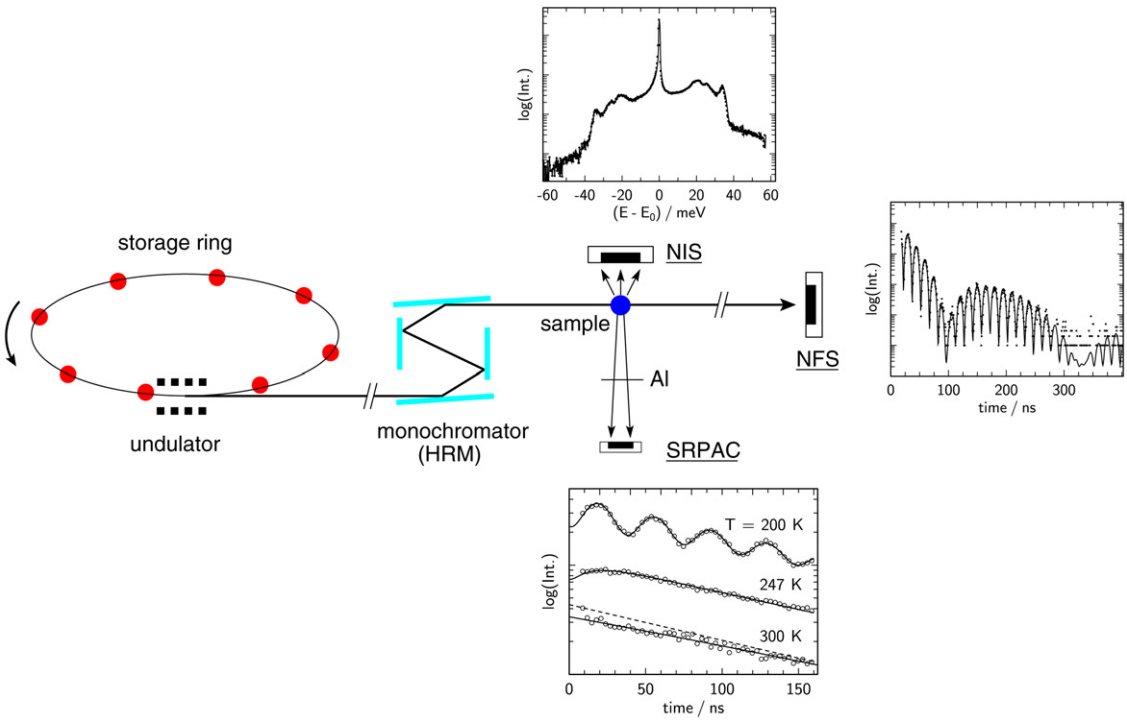

Fig. 1. Scheme of the setup for some techniques in NRS: NFS (NQES, NSAS, GINRS), NIS, and SRPAC. Furthermore, the corresponding time and energy spectra are schematically shown measured by the detectors for NFS, SRPAC and NIS. The storage ring is operated in 'few bunch' mode with e.g. 176 ns spacing between adjacent buckets (bullets). The undulator produces the well-collimated synchrotron radiation which is monochromized at the nuclear resonances by a high resolution monochromator, HRM (bandwidth $\Delta E \approx$ meV). Finally, the radiation impinges the sample. Depending on the scattering process and the scattering geometry different techniques can simultaneously be exploited. Variable sample environments allow for the combination of high/low temperature, high pressure, and external magnetic field.

Nuclear resonance scattering makes full use of the outstanding properties of third generation synchrotron radiation sources and being a resonant X-ray scattering technique in the time domain, it relies on the well-defined time structure of this source. It is based on the Mössbauer effect and the scattering proceeds via the Mössbauer level. An X-ray pulse from a synchrotron radiation source which is very sharp in time ($\sim$100 ps) and very broad in energy (white radiation) is exciting the nuclear levels in the sample and creates a 'coherent collective nuclear state'. The successive decay of these levels gives rise to an exponential intensity decay in time determined by the lifetime τ_0 of the involved nuclear level, which is generally much larger than the synchrotron radiation pulse. Utilizing proper detector schemes one gets practically a background free spectroscopy.

Various techniques are used, as shown in Fig. 1: nuclear forward scattering (NFS) [1,2], nuclear quasi-elastic scattering (NQES) [3], nuclear Bragg diffraction (NBD) [4–6], nuclear reflectometry or grazing incidence nuclear resonance scattering (GINRS, for the investigation of surfaces and multilayers) [7–10], nuclear small angle scattering (NSAS, measuring e.g. magnetic domain structures) [11,12], nuclear inelastic scattering (NIS) [13–15], and synchrotron radiation based perturbed angular correlation (SRPAC) [16,17].

A detailed review on the method and theory has recently been published [18] as well as on applications to solid state physics [19].

In the following sections we will give some typical examples from investigations at the ESRF where the technique comes to its own: high pressure, nano-scale materials, and dynamics of disordered systems.

2. Applications to high pressure

High pressure applications are one of the domains which benefit most from the outstanding properties of synchrotron radiation. The small beam size allows one to work with samples as small as 25 μm in diameter. In this case,

state-of-the-art diamond anvil cells (DAC) are able to reach pressures far above the 100 GPa regime, up to 300 GPa; those pressures which are common in the center of the Earth. In combination with laser heating (5000 K) access to the entire relevant (pressure, temperature)-space becomes available. First applications have been reported for iron containing specimens [20,21]. Furthermore, the small divergence of the beam allows sophisticated sample environments, in situ pressure calibration and diffraction studies not only for the determination of the induced volume change with pressure but also to identify phase transitions. The following two examples demonstrate typical applications. In the first example iron metal has been investigated by NFS and NIS in order to follow over the pressure induced phase transition magnetic order (via the hyperfine field) and structural dynamics (via the (partial) vibrational density of states, DOS) and in the second example the long standing quest for the magnetic phase in SmS under applied pressure has been tackled.

2.1. Iron metal

Recently, the high pressure behaviour of iron gained much interest due to unusual superconductivity, to simulations of the inner core of the Earth, and to improved technical developments in high pressure research. It is well known that α-iron undergoes under pressure a magnetic and structural phase transition to the hexagonal closed-packed (hcp) phase of iron (ϵ-iron) in the pressure range of 10 to 22 GPa at ambient temperature.

A 2.5 μm thick iron foil enriched to 95% in ^{57}Fe was pressurized in a DAC [22]. Fig. 2 shows the NFS spectra for various pressures. At 3 GPa the spectrum reveals iron in the pure α-phase witnessed by the regular quantum beat pattern from the internal hyperfine field of 33 T. At 14 GPa the influence of the ϵ-phase is already quite pronounced. With a further increase in pressure the influence of the non-magnetic ϵ-phase becomes dominant. At 21 GPa the sample is almost completely in the ϵ-phase. Now the NFS spectrum is modified only by a single Bessel minimum at 50 ns which originates from the increased effective thickness in comparison to that of the magnetically split one.

With the same sample, NIS energy dependencies have been recorded and the vibrational densities of states have been extracted [23]. Examples at ambient pressure and at 42 GPa are displayed in Fig. 3. All spectral features of the DOS of ϵ-Fe are shifted to higher energies with respect to α-Fe revealing a hardening of the lattice vibrations.

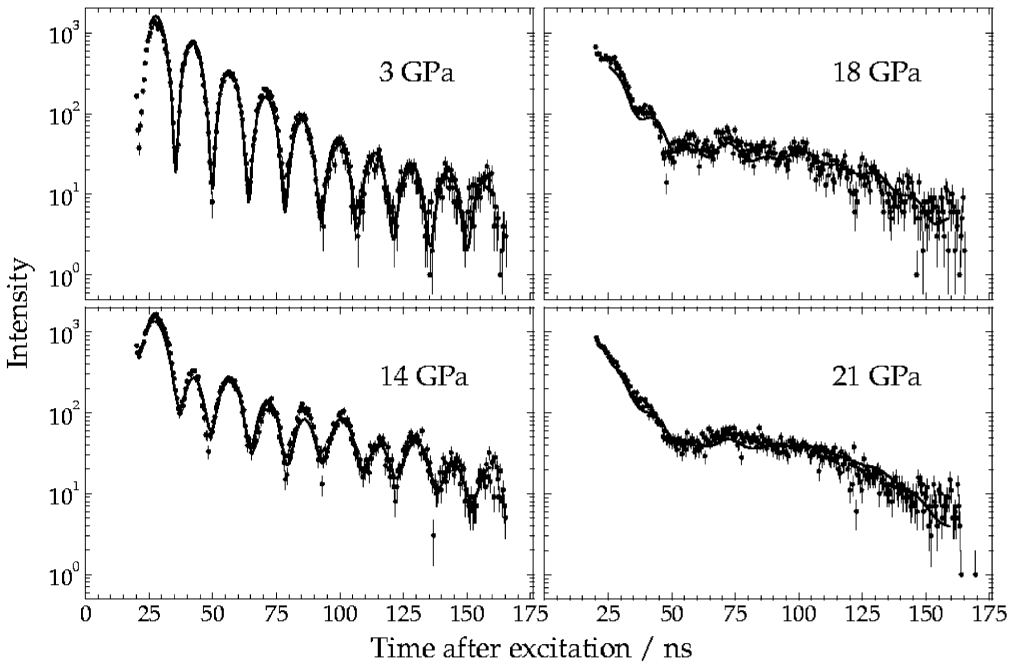

Fig. 2. Time spectra of NFS from the pressure induced $\alpha \rightarrow \epsilon$ transition in Fe at various pressures (from [22]).

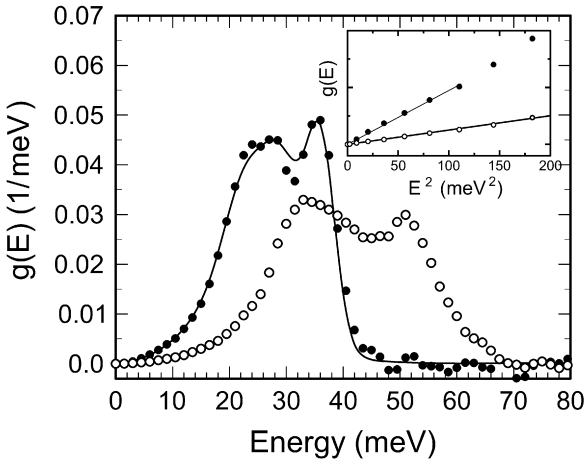

Fig. 3. Phonon density of states from the pressure induced $\alpha \rightarrow \epsilon$ transition in Fe at ambient pressure (solid circles) and 42 GPa (open circles). The solid line represents the DOS from neutron scattering. The inset displays the corresponding low energy part for the determination of sound velocities (from [23]). Here the solid lines represent a linear fit to the data.

Several thermodynamical properties have been derived as the Lamb–Mössbauer factor, f_{LM} and the mean-square displacement, respectively, the mean phonon energy and the corresponding Debye temperature, the lattice contribution to the specific heat c_{V}, the internal energy, entropy and the mean force constant. Finally, from the low-energy part of the density of phonon states the average velocity of sound v_{av} (Fig. 3 insert) has been derived according to the relation

$$g(E) = \frac{V}{2\pi^2\hbar^3 v_{\mathrm{av}}^3} E^2 \tag{1}$$

with V the volume per Fe atom. Extensions to higher pressures have been reported [24] and investigations to account for anisotropies [25,26]. These sound velocity data have been complemented by recent data from inelastic X-ray scattering [27] and in the very high pressure regime by those from shock waves [28].

2.2. Magnetic order in SmS

Recently, magnetic quantum critical points (QCPs) have attracted much interest, especially after the discovery of the appearance of unconventional superconductivity at a QCP and of the causative role of spin and charge fluctuations.

One class of systems known as Kondo insulators deserves special attention. Among them, SmS is known to be a non-magnetic (Sm^{2+}) semiconductor at ambient pressure (black phase). It becomes metallic (golden phase) under pressure (0.65 GPa at room temperature), at which the Sm ions are in an intermediate valence state. So far it has been considered that, by increasing further the pressure, the golden phase could evolve into a magnetic state where the Sm ions are trivalent (Sm^{3+}). However, to date there has been no clear evidence of it.

Fig. 4 shows the pressure dependence of the hyperfine parameters (magnetic hyperfine field B_{hf} and electric quadrupole splitting ΔE_Q) and of the magnetic component fraction at 3 K [29]. The pressure-induced phase transition from a non-magnetic state into a magnetically-ordered state at $p_c \sim 2$ GPa is evident. The steep variation of both B_{hf} and ΔE_Q as well as the coexistence of the low and high-pressure phases in the vicinity of p_c point towards a first-order transition. The absolute values of B_{hf} and ΔE_Q are consistent with the occurrence of a Γ_8 crystal field ground state for the Sm^{3+} ions, with a magnetic moment of the order of 0.5 μ_B. The high-pressure magnetically-ordered phase is stable up to at least 19 GPa, as shown by the very weak pressure dependence of the hyperfine parameters and by the increase with pressure of the ordering temperature T_m. These results give the first direct evidence that a magnetic ground state appears for SmS at a pressure of 2 GPa. Surprisingly, at this pressure the valence is about 2.8 and reaches the trivalent state only at about 13 GPa [30] without any visible change in the magnetic properties.

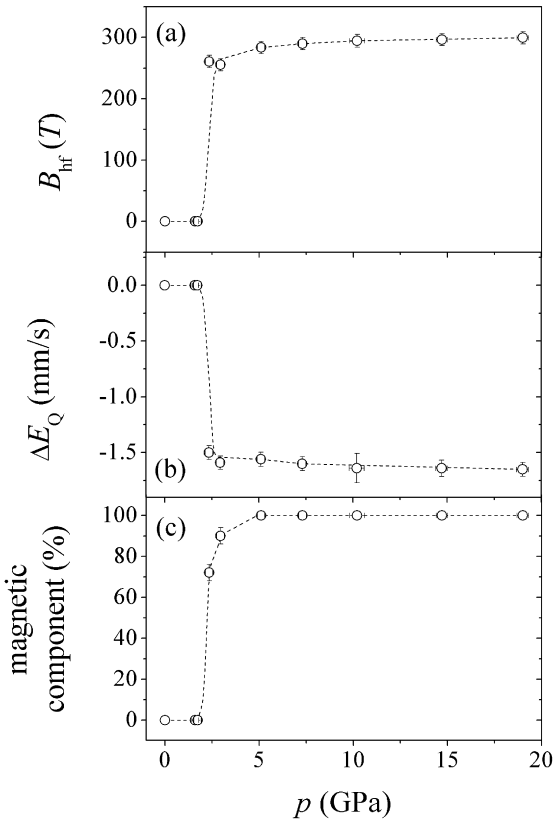

Fig. 4. Pressure dependence for SmS of (a) the magnetic hyperfine field (B_{hf}), (b) the electric quadrupole splitting (ΔE_Q), and (c) the magnetic component fraction at $T = 3$ K. The dashed lines through the data points are guides to the eye. (Figure taken from [45].)

3. Applications to nano-scale materials

3.1. Dynamics of nano-crystalline material

Fast and slow dynamics, i.e., vibrational dynamics and diffusion, in amorphous, low-dimensional and nanostructured solids is a rapidly growing research field. Atomic diffusion governs the structural relaxation and associated changes in the physical properties whereas vibrational dynamics becomes crucial in thermodynamic, conductive, and optical properties of mesoscopic systems.

3.1.1. Scale effects on the vibrational properties of nanocrystalline iron

A wealth of novel phenomena, such as phonon folding, phonon confinement, and vibrational interface states have been revealed in the last few years. A key role in this respect is played by the vibrational density of states, $g(E)$. In the DOS of nanocrystalline (NC) materials, i.e., polycrystals with an ultrafine grain size d, both finite-size effects and interface-related phenomena due to the large fraction of disordered interfaces are expected. In particular, two basic questions are extremely relevant: (i) how does the DOS scale with d, and (ii) is there a deviation from the usual Debye law $g(E) = a \cdot E^2$ at low energies?

Nuclear inelastic scattering of synchrotron radiation was applied to the determination of the DOS in NC iron samples with different grain size, prepared by inert gas condensation [31]. The oxidation degree of the samples $(1 - x)$ is defined as the atomic fraction of oxidised Fe atoms, obtained from X-ray diffraction and Mössbauer spectroscopy. In the NC samples, in comparison with a reference α-Fe foil, an enhanced population of low-energy modes and a broadening of the longitudinal peak at about 36 meV were observed (Fig. 5). This softening can be explained only partially by oxidation of the grain interfaces: a linear combination $x \cdot g_{\alpha\text{-Fe}} + (1 - x) \cdot g_{\text{oxide}}$ does not fully account for the low-energy intensity. Here $g_{\alpha\text{-Fe}}$ and g_{oxide} is the DOS measured for α-Fe and totally oxidised nanoparticles,

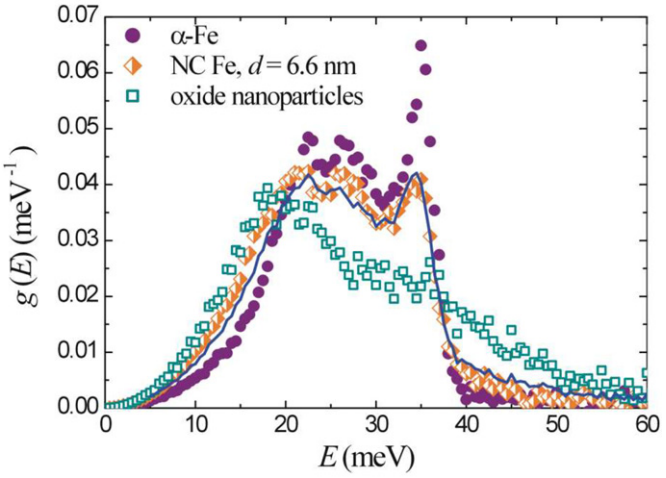

Fig. 5. DOS of NC iron ($d = 6.6$ nm), iron oxide nanoparticles, and reference α-iron. Solid line: linear combination $x \cdot g_{\alpha\text{-Fe}} + (1 - x) \cdot g_{\text{oxide}}$ after convoluting $g_{\alpha\text{-Fe}}$ with a 1.1 meV FWHM Lorentzian in order to represent phonon damping. (Figure taken from [46].)

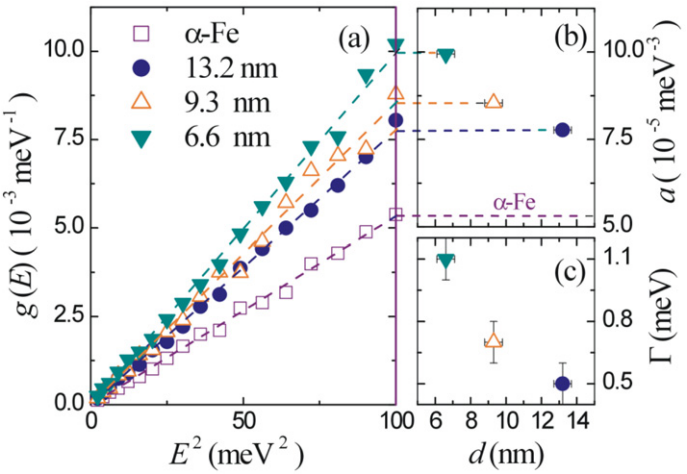

Fig. 6. (a) Low-energy DOS versus energy square of NC samples with different grain size. Dashed lines: best fits according to $g(E) = a \cdot E^2$; (b), (c) coefficient a and damping parameter Γ versus grain size, respectively. (Figure taken from [46].)

respectively. The remaining excess modes are most likely ascribable to vibrations of atoms at the grain interfaces, with modified local environment and softened force constants. Most notably, the low-energy DOS exhibits a $g(E) = a \cdot E^2$ dependence over the whole range 1.5–15 meV for all measured samples (Fig. 6(a)), and the coefficient a increases with decreasing d (Fig. 6(b)).

3.1.2. Iron self-diffusion in nanocrystalline alloys

With the newly developed method of nuclear resonance reflectivity using nuclear resonance scattering from isotopic multilayers the study of self-diffusion of Mössbauer isotopes over a wide range of diffusivity, 10^{-26} m^2 s^{-1} to 10^{-18} m^2 s^{-1}, became feasible [10]. At the same time, this technique is sensitive enough to measure diffusion lengths as small as 0.1 nm, which is more than an order of magnitude larger than the sensitivity of conventional depth profiling techniques. Fig. 7 shows nuclear resonance reflectivity of isotopic multilayer of nanocrystalline FeNZr having structure [^{57}FeNZr (4 nm)/FeNZr (3 nm)]$_{20}$. The film is chemically homogeneous, however, scattering contrast between adjacent layers emanates due to the nuclear resonance scattering from the ^{57}Fe isotope. A Bragg peak around $q_z = 0.9$ nm^{-1} is observed due to isotopic periodicity. As the multilayer is annealed, iron atoms diffuse across the isotopic interfaces, and the intensity of the Bragg peak decays with annealing time, yielding the diffusion length through

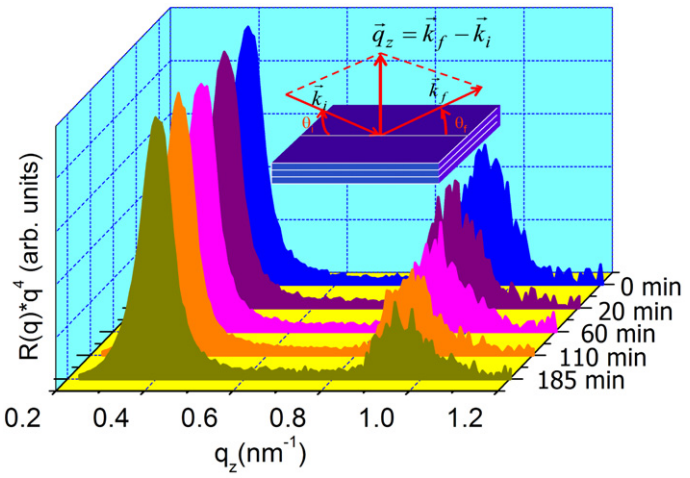

Fig. 7. Nuclear resonance reflectivity of the $[^{57}\text{FeNZr (4 nm)/FeNZr (3 nm)}]_{20}$ multilayer as a function of annealing time at 393 K. (Figure taken from [47].) The peaks at $q_z \sim 0.5$ nm^{-1} are the 'total reflection peaks' and those at $q_z \sim 0.9$ nm^{-1} the 1st order Bragg peaks. The latter diminish in time as the ^{57}Fe atoms diffuse through the multilayer structure.

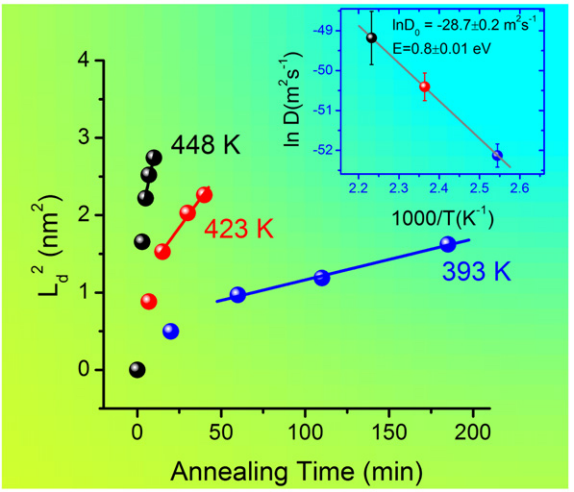

Fig. 8. Evolution of interdiffusion length L_d as a function of annealing time at different temperatures. The insert shows the Arrhenius behaviour of the diffusion coefficient with isothermal annealing temperature, yielding the activation energy and pre-exponent factor for self-diffusion of Fe. (Figure taken from [47].)

the relation, $\ln[I(t)/I(0)] = -4\pi^2 n^2 L_d^2/d^2$, where $I(t)$ is the intensity of the Bragg peak after annealing time t, n is the order of Bragg reflection, L_d is the diffusion length and d is the bilayer periodicity. Fig. 8 gives L_d as a function of annealing time at three different temperatures T. It increases initially at a faster rate and after a certain annealing time the rate becomes constant. The initial faster increase in the diffusion length is associated with the structural relaxation in the system, similar to amorphous alloys. This relaxation is associated with the relaxation of the highly disordered grain boundary region, stress relaxation in the film and annealing out of the defects inside the nanocrystals. After sufficiently long annealing time, the diffusion length increases linearly with annealing time and the diffusivity was obtained by a linear fit using the relation: $L_d^2 = 2 \cdot D(T) \cdot t$. The diffusivity follows Arrhenius type behaviour with temperature, as shown in the inset of Fig. 8. The solid line in the figure is a fit to the experimental data obtained using the relation $D = D_0 \exp(-E/k_B T)$, where E is the activation energy and D_0 is the pre-exponential factor which contains the details of the diffusion mechanism. The activation energy for self-diffusion of Fe in the present system is significantly lower than that in the amorphous FeN of similar composition. This result is in general agreement with the earlier studies where the low activation energy for diffusion in nanocrystalline alloys has been attributed to a higher

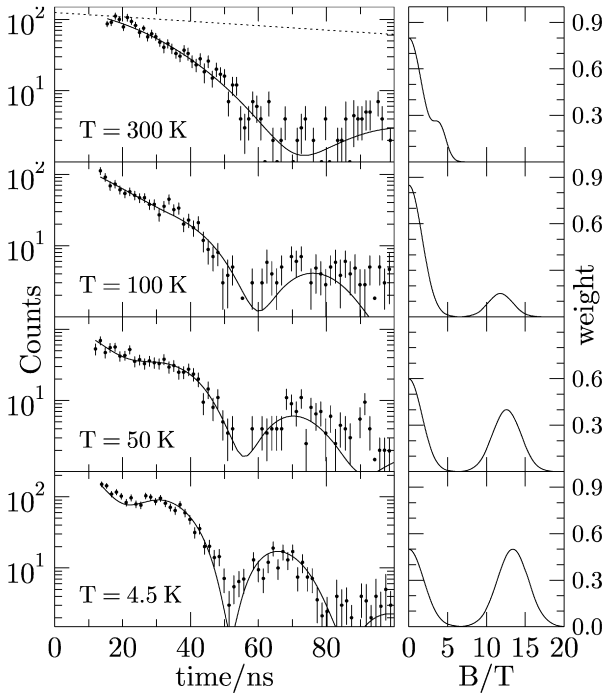

Fig. 9. Time spectra of nuclear resonant grazing-incidence reflection from ultrasmall ^{57}Fe islands on W (110). The modulation of the intensity is attributed to a perpendicular magnetization of the Fe islands. The solid lines are the results of simulations. The right panel displays the probability density for the hyperfine field distribution that was obtained from the simulations. (Figure taken from [48].)

density of grain boundaries. Further, the observed values of D_0 and E suggest that the mechanism of diffusion in this system is similar to that in amorphous alloys.

3.2. Magnetism of nano-structured material

The understanding of magnetism of self organized nano-structures and clusters gained much attention because of fundamental aspects of nanoscale magnetic ordering in general and possible applications in high-density magnetic storage and magnetoelectronics.

3.2.1. Iron on W (110)

As an example the perpendicular spin orientation in ultra small Fe islands on W (110) will be discussed [8]. Ultra small pseudomorphic Fe islands on an atomically clean W (110) crystal have been prepared by thermal evaporation of Fe enriched to 95% in ^{57}Fe. The coverage of the Fe islands was 0.57 which is slightly below the percolation limit. Their average diameter was determined to be 2.0 nm. A coating of five monolayers of Ag prevents the sample from contamination. Fig. 9 left panel displays the time spectra taken in grazing incidence geometry between 300 and 4.5 K. The right panel of Fig. 9 shows the weight of the magnetic component. It increases with decreasing temperature. This can be attributed to superparamagnetic relaxation of the magnetic moments. At high temperatures the magnetization of small particles is subject to fast thermal fluctuations so that the effective magnetic hyperfine field averages to zero. The transition from the fast relaxation regime to the magnetically ordered state occurs at about 50 K, however, it is a very broad transition certainly due to the size distribution of the islands. The modulation in the time spectra is characteristic for a perpendicular magnetization. This result is quite remarkable because Fe films on W (110) are known to be magnetized in plane for coverages of more than 0.6.

3.2.2. Exchange-coupled thin films

Exchange-coupling between soft- and hard-magnetic phases plays an important role in the engineering of novel functional magnetic nanostructures. There exist some micromagnetical models describing this behaviour, however,

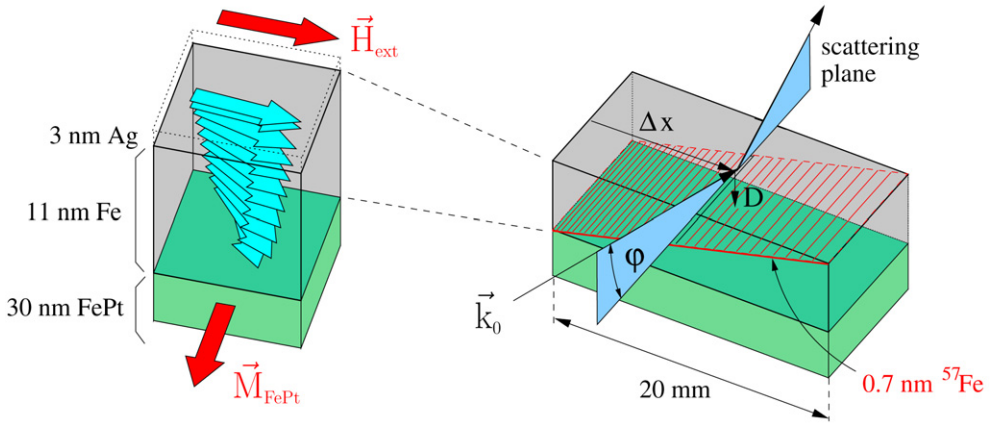

Fig. 10. Magnetic structure in the iron layer of an Fe/FePt exchange spring as it forms in an external magnetic field $\vec{H}_{ext}$ of 160 mT. This image was obtained using an ultrathin probe layer embedded in the iron film, shown on the right (figure taken from [49]).

due to methodological difficulties there exist nearly no direct measurements of the actual spin structure. Utilizing the technique of probe layers, i.e. inserting ^{57}Fe in various depths of the thin iron film (see Fig. 10 right panel), NRS directly probes the actual spin structure in various depths by selectively exciting the ^{57}Fe layer at various lateral positions [9]. The sample investigated here is a bilayer system consisting of 11 nm Fe on 30 nm $Fe_{55}Pt_{45}$ in the hard-magnetic tetragonal $L1_0$ phase. A wedge-shaped 0.7 nm thick ^{57}Fe film with a slope of 0.5 nm/mm has been produced. Different depths D in the sample can thus be probed by adjusting the displacement Δx of the sample transversely to the incident beam. The sample was magnetically saturated in an external field of 2.3 T so that the remanent magnetization $\vec{M}_{FePt}$ of the $Fe_{55}Pt_{45}$ layer was oriented along $\vec{k}_0$, as shown in Fig. 10. Time spectra at 4 K with selected in-plane external fields $\vec{H}_{ext}$ perpendicular to $\vec{k}_0$ were taken at various displacements Δx. Evaluation of the spectra reveals the depth dependence of the rotation of the magnetization in the iron film with atomic resolution (see Fig. 10 left panel).

4. Dynamics of disordered systems

NRS techniques are well suited for the investigation of the dynamics of disordered systems over a huge time scale. Whereas NIS covers the fast regime of phonons, NQES techniques complement the investigations to the slow time regime (10^5–10^{10} Hz). Furthermore, the technique of probe molecules allows for the investigation of glasses, which do not contain Mössbauer atoms and, when carefully chosen, allows for mode selectivity as collective and non-collective modes, respectively, and translational and rotational relaxations, respectively.

The following two examples cover both aspects, fast dynamics of glasses with emphasis to the so-called 'boson peak' and the nature of α- and slow β-relaxation in the glass former dibutyl phthalate (DBP).

4.1. Universal dynamics of glass

Glass dynamics has been studied since decades and the boson peak more than 30 years. However, the nature of it is still debated. NIS allowed for the first time to study selectively collective modes utilizing the technique of 'probe molecules'. The probes, which are molecules with a resonant (Mössbauer) nucleus in the centre of mass 'swims' in a glass matrix without coupling to the host molecules. It follows the collective motions of the glass without being sensitive to the local modes of the host molecule. Furthermore, one selects pure translational motions of the probes: rotation is disregarded because the spectator nucleus is in the centre of mass; the few intra-molecular modes are separated in energy. The selected pure translational motions of the probe give the 'density of states of collective motions' (CDOS) of the glass matrix. For all studied glasses, the reduced CDOS $g(E)/E^2$ clearly exhibits an excess of low-energy modes, the boson peak, which is shown exemplarily for ferrocene in DBP in Fig. 11 left panel. The positions of the peak are consistent with the boson peak energies in the total DOS from neutron scattering data. The temperature evolution of the boson peak shows the same features as observed with other methods. This clear

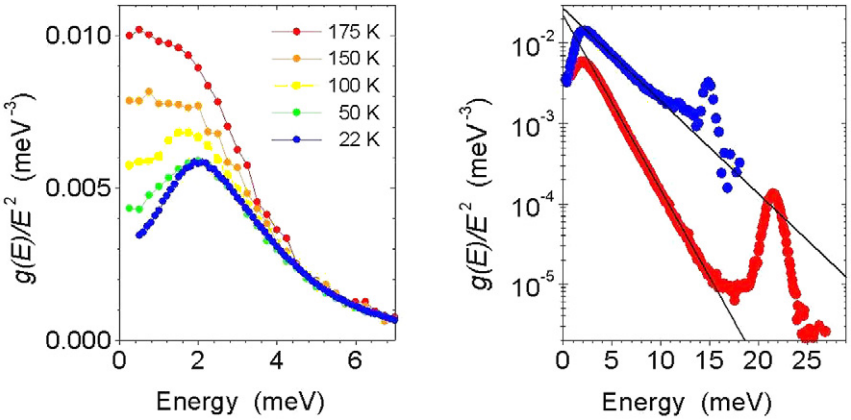

Fig. 11. Left panel: Temperature dependence of the reduced DOS of collective motions of ferrocene in dibutyl phthalate. Right panel: Reduced DOS of collective motions of ferrocene in DBP from NIS measurements (lower curve) and of pure DBP from neutron measurements (upper curve). The neutron data are scaled to match the NIS data at lowest energy. Solid lines show the fit according to the equation (see text). (Figure taken from [50].)

manifestation of the boson peak in the CDOS proves that the boson peak in the total DOS is largely composed of collective modes. Beyond the boson peak, the reduced density of states of collective motions reveals a temperature-independent exponential behaviour: $g(E)/E^2 \propto \exp(-E/E_0)$, which was not reported earlier. On a logarithmic scale, $g(E)/E^2$ follows a straight line over three decades of the reduced CDOS and deviates only when obscured by the eigen mode of ferrocene at 22 meV (Fig. 11 right panel). We also found this exponential behaviour in the total DOS available from neutron data [32]. Further investigations towards the understanding of the boson peak have been carried out on hyperquenched [33] and on densified glasses [34]. All these results suggest that for a glass with a given microscopic structure the transformation of atomic vibrations is sufficiently described by the corresponding transformation of the elastic medium.

4.2. α- and β-relaxation

Approaching the slow time regime relaxation times and transport properties of moderately supercooled liquids exhibit a universal dependence on temperature. At the glass transition temperature, T_g, the relaxation of organic glass formers usually splits into two processes, the α-relaxation, which corresponds to cooperative molecular dynamics, and the slow β-relaxation, which microscopic origin is still disputed. NRS techniques may shine some more light in the underlaying mechanism. The above studied DBP with the probe molecule ferrocene ($T_g = 178$ K) was investigated by NFS (sensitive to translational and rotational dynamics) and SRPAC (sensitive only to rotational dynamics) [17]. NFS spectroscopy is applicable as long as the Lamb–Mössbauer factor f_{LM} is greater than zero which holds in this case up to 210 K. SRPAC on the other hand does not depend on f_{LM} and can be applied in the entire temperature regime. At the lower temperatures, the SRPAC intensity follows an exponential decay modulated by quantum beats. In the regime of slow relaxation, the beats are damped at a rate proportional to rotational relaxation. Similar quantum beats modulate the decay of the NFS intensity, where the damping depends on the sum of rotational and translational relaxation. At higher temperatures, in the regime of fast relaxation, only SRPAC spectra can be measured. From the measured time spectra relaxation rates have been determined (see Fig. 12). Below 190 K the data sets from both techniques coincide, which means that translational dynamics is absent in the experimental time window. Above 190 K the NFS data begin to deviate from the SRPAC data because translational dynamics is activated. From these results the pure translational relaxation rates have been derived. Comparing the NRS relaxation rates with data of pure DBP as obtained from dielectric spectroscopy (DS), we may now interpret those two branches in DS at low temperature. The branch of slow β-relaxation follows the NRS data of rotational dynamics, whereas the branch of α-relaxation decreases in parallel with the NRS data of translational dynamics. This correlation suggest a decoupling and, especially, that the slow β-relaxation is connected with rotational dynamics.

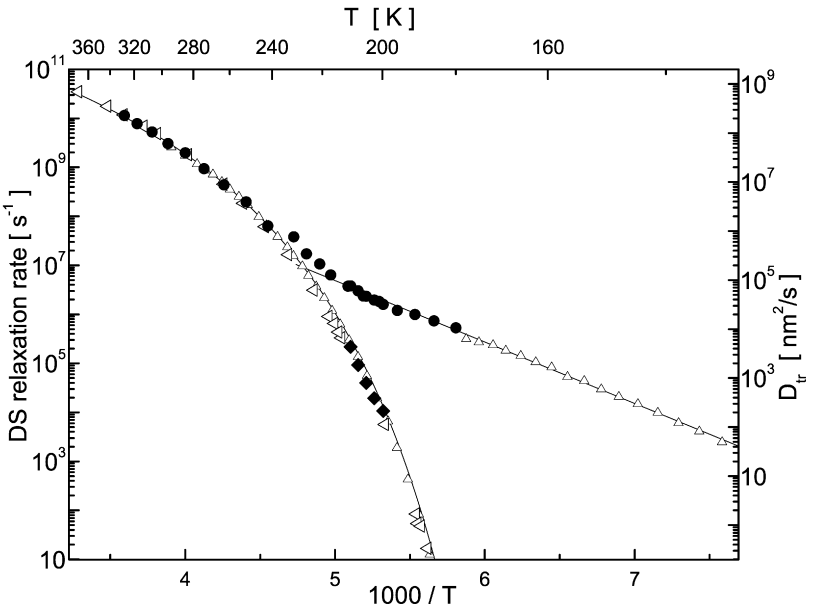

Fig. 12. Comparison of the rotational relaxation rate of the ferrocene molecule in DBP (glass temperature $T_G = 178$ K) derived from SRPAC (●) and the translational relaxation rate derived from NFS (◆) to the DS data [51] for pure DBP (▷). The solid lines are fits to the DS data by Vogel–Fulcher and Arrhenius functions, respectively. (Figure taken from [52].)

5. Further applications and summary

In the previous sections selected topics have been presented. Others could not be mentioned, such as investigations of biological relevant samples which became a growing field with emphasis to their dynamic and electronic properties (see e.g. [35–37]) or thermoelectric materials [38,39]. The outstanding energy resolution and the timing properties of NRS led to applications beyond spectroscopy. Contributions to the definition of the length scale [40], correlation behaviour [41], interferometry [42,43], and the utilisation of waveguides [44] show the hole breath of the method. All those applications became possible with the advent of powerful synchrotron radiation sources around the world as APS (Argonne, USA), SPring-8 (Harima, Japan), and ESRF (Grenoble, France). Nowadays nuclear resonance scattering techniques matured to a spectroscopy with unique applications in various fields. The probe molecule/layer technique, the application of sophisticated sample environments, and the possibility to apply simultaneously various NRS techniques and other techniques makes this spectroscopy an unique tool. The previous typical examples demonstrate the versatility and huge potential of the technique.

References

[1] J.B. Hastings, D.P. Siddons, U. van Bürck, R. Hollatz, U. Bergmann, Mössbauer spectroscopy using synchrotron radiation, Phys. Rev. Lett. 66 (6) (February 1991) 770–773.

[2] U. van Bürck, D.P. Siddons, J.B. Hastings, U. Bergmann, R. Hollatz, Nuclear forward scattering of synchrotron radiation, Phys. Rev. B 46 (10) (September 1992) 6207–6211.

[3] B. Sepiol, A. Meyer, G. Vogl, R. Rüffer, A.I. Chumakov, A.Q.R. Baron, Time domain study of ^{57}Fe diffusion using nuclear forward scattering of synchrotron radiation, Phys. Rev. Lett. 76 (17) (April 1996) 3220–3223.

[4] E. Gerdau, R. Rüffer, H. Winkler, W. Tolkdorf, C.P. Klages, J.P. Hannon, Nuclear Bragg diffraction of synchrotron radiation in yttrium iron garnet, Phys. Rev. Lett. 54 (February 1985) 835–838.

[5] R. Rüffer, E. Gerdau, R. Hollatz, J.P. Hannon, Nuclear Bragg scattering of synchrotron radiation pulses in a single-reflection geometry, Phys. Rev. Lett. 58 (22) (June 1987) 2359–2362.

[6] U. van Bürck, R.L. Mössbauer, E. Gerdau, R. Rüffer, R. Hollatz, G.V. Smirnov, J.P. Hannon, Nuclear Bragg scattering of synchrotron radiation with strong speedup of coherent decay, measured on antiferromagnetic $^{57}FeBO_3$, Phys. Rev. Lett. 59 (3) (July 1987) 355–358.

[7] L. Niesen, A. Mugarza, M.F. Rosu, R. Coehoorn, R.M. Jungblut, F. Roozeboom, A.Q.R. Baron, A.I. Chumakov, R. Rüffer, Magnetic behavior of probe layers of ^{57}Fe in thin Fe films observed by means of nuclear resonant scattering of synchrotron radiation, Phys. Rev. B 58 (13) (October 1998) 8590–8595.

[8] R. Röhlsberger, J. Bansmann, V. Senz, K.L. Jonas, A. Bettac, O. Leupold, R. Rüffer, E. Burkel, K.H. Meiwes-Broer, Perpendicular spin orientation in ultrasmall Fe islands on W(110), Phys. Rev. Lett. 86 (24) (June 2001) 5597–5600.
[9] R. Röhlsberger, H. Thomas, K. Schlage, E. Burkel, O. Leupold, R. Rüffer, Imaging the magnetic spin structure of exchange-coupled thin films, Phys. Rev. Lett. 89 (23) (November 2002) 237201.
[10] A. Gupta, M. Gupta, S. Chakravarty, R. Rüffer, H.-C. Wille, O. Leupold, Fe diffusion in amorphous and nanocrystalline alloys studied using nuclear resonance reflectivity, Phys. Rev. B 72 (1) (July 2005) 014207.
[11] Yu.V. Shvyd'ko, A.I. Chumakov, A.Q.R. Baron, E. Gerdau, R. Rüffer, A. Bernhard, J. Metge, Nuclear resonance small-angle scattering of X rays, Phys. Rev. B 54 (21) (December 1996) 14942–14945.
[12] D.L. Nagy, L. Bottyán, B. Croonenborghs, L. Deák, B. Degroote, J. Dekoster, H.J. Lauter, V. Lauter-Pasyuk, O. Leupold, M. Major, J. Meersschaut, O. Nikonov, A. Petrenko, R. Rüffer, H. Spiering, E. Szilágyi, Coarsening of antiferromagnetic domains in multilayers: The key role of magnetocrystalline anisotropy, Phys. Rev. Lett. 88 (15) (March 2002) 157202.
[13] M. Seto, Y. Yoda, S. Kikuta, X.W. Zhang, M. Ando, Observation of nuclear resonant scattering accompanied by phonon excitation using synchrotron radiation, Phys. Rev. Lett. 74 (19) (May 1995) 3828–3831.
[14] W. Sturhahn, T.S. Toellner, E.E. Alp, X.W. Zhang, M. Ando, Y. Yoda, S. Kikuta, M. Seto, C.W. Kimball, B. Dabrowski, Phonon density of states measured by inelastic nuclear resonant scattering, Phys. Rev. Lett. 74 (May 1995) 3832–3835.
[15] A.I. Chumakov, R. Rüffer, H. Grünsteudel, H.F. Grünsteudel, G. Grübel, J. Metge, O. Leupold, H.A. Goodwin, Energy dependence of nuclear recoil measured with incoherent nuclear scattering, Europhys. Lett. 30 (February 1995) 427–430.
[16] A.Q.R. Baron, A.I. Chumakov, R. Rüffer, H. Grünsteudel, H.F. Grünsteudel, O. Leupold, Single-nucleus quantum beats excited by synchrotron radiation, Europhys. Lett. 34 (5) (1996) 331–336.
[17] I. Sergueev, U. van Bürck, A.I. Chumakov, T. Asthalter, G.V. Smirnov, H. Franz, R. Rüffer, W. Petry, Synchrotron-radiation-based perturbed angular correlations used in the investigation of rotational dynamics in soft matter, Phys. Rev. B 73 (2) (January 2006) 024203.
[18] E. Gerdau, H. de Waard (Eds.), Nuclear Resonant Scattering of Synchrotron Radiation, Hyperfine Interactions, vol. 123–125, Baltzer Science Publishers, 1999/2000.
[19] R. Röhlsberger, Nuclear Condensed Matter Physics with Synchrotron Radiation—Basic Principles, Methodology and Applications, Springer Tracts in Modern Physics, vol. 208, Springer Publishers, 2004.
[20] J. Zhao, W. Sturhahn, J.F. Lin, G. Shen, E.E. Alp, H.K. Mao, Nuclear resonant scattering at high pressure and high temperature, High Pressure Res. 24 (2004) 447–457.
[21] J.F. Lin, W. Sturhahn, J.Y. Zhao, G.Y. Shen, H.K. Mao, R.J. Hemley, Absolute temperature measurement in a laser-heated diamond anvil cell, Geophys. Res. Lett. 31 (2004) L14611.
[22] H.F. Grünsteudel, Der α-ϵ-Übergang in Eisen als Beispiel für nukleare Vorwärtsstreuung von Synchrotronstrahlung an Proben unter hohem Druck, PhD thesis, Universität Paderborn, Paderborn, 1997.
[23] R. Lübbers, H.F. Grünsteudel, A.I. Chumakov, G. Wortmann, Density of phonon states in iron at high pressure, Science 287 (February 2000) 1250–1252.
[24] H.K. Mao, J. Xu, V.V. Struzhkin, J. Shu, R.J. Hemley, W. Sturhahn, M.Y. Hu, E.E. Alp, L. Vocadlo, D. Alfé, G.D. Price, M.J. Gillan, M. Schwoerer-Böhning, D. Häusermann, P. Eng, G. Shen, H. Giefers, R. Lübbers, G. Wortmann, Phonon density of states of iron up to 153 gigapascal, Science 292 (May 2001) 914–916.
[25] R. Lübbers, H. Giefers, K. Rupprecht, G. Wortmann, A.I. Chumakov, High-pressure phonon spectroscopy of oriented hcp iron. ESRF Highlights 2000, February 2001, pp. 48–49.
[26] H. Giefers, R. Lübbers, K. Rupprecht, G. Wortmann, D. Alfe, A.I. Chumakov, Phonon spectroscopy of oriented hcp iron, High Pressure Res. 22 (May 2002) 501–506.
[27] D. Antonangeli, F. Occelli, H. Requardt, J. Badro, G. Fiquet, M. Krisch, Elastic anisotropy in textured hcp-iron to 112 GPa from sound wave propagation measurements, Earth Planetary Sci. Lett. 225 (1–2) (August 2004) 243–251.
[28] J.M. Brown, R.G. McQueen, Phase transitions, Grüneisen parameter and elasticity for shocked iron between 77 GPa and 400 GPa, J. Geophys. Res. 91 (1986) 7485–7494.
[29] A. Barla, J.P. Sanchez, Y. Haga, G. Lapertot, B.P. Doyle, O. Leupold, R. Rüffer, M.M. Abd-Elmeguid, R. Lengsdorf, J. Flouquet, Pressure-induced magnetic order in golden SmS, Phys. Rev. Lett. 92 (6) (February 2004) 066401.
[30] E. Annese, A. Barla, C. Dallera, G. Lapertot, J.-P. Sanchez, G. Vankó, Divalent-to-trivalent transition of Sm in SmS: Implications for the high-pressure magnetically ordered state, Phys. Rev. B 73 (14) (April 2006) 140409.
[31] L. Pasquini, A. Barla, A.I. Chumakov, O. Leupold, R. Rüffer, A. Deriu, E. Bonetti, Size and oxidation effects on the vibrational properties of nanocrystalline α-Fe, Phys. Rev. B 66 (7) (August 2002) 073410.
[32] A.I. Chumakov, I. Sergueev, U. van Bürck, W. Schirmacher, T. Asthalter, R. Rüffer, O. Leupold, W. Petry, Collective nature of the boson peak and universal transboson dynamics of glasses, Phys. Rev. Lett. 92 (24) (June 2004) 245508.
[33] A. Monaco, A.I. Chumakov, Y.-Z. Yue, G. Monaco, L. Comez, D. Fioretto, W.A. Crichton, R. Rüffer, Density of vibrational states of a hyperquenched glass, Phys. Rev. Lett. 96 (20) (May 2006) 205502.
[34] A. Monaco, A.I. Chumakov, G. Monaco, W.A. Crichton, A. Meyer, L. Comez, D. Fioretto, J. Korecki, R. Rüffer, Effect of densification on the density of vibrational states of glasses, Phys. Rev. Lett. 97 (13) (September 2006) 135501.
[35] J.T. Sage, S.M. Durbin, W. Sturhahn, D.C. Wharton, P.M. Champion, P. Hession, J. Sutter, E.E. Alp, Long-range reactive dynamics in myoglobin, Phys. Rev. Lett. 86 (21) (May 2001) 4966–4969.
[36] K. Achterhold, C. Keppler, A. Ostermann, U. van Bürck, W. Sturhahn, E.E. Alp, F.G. Parak, Vibrational dynamics of myoglobin determined by the phonon-assisted Mössbauer effect, Phys. Rev. E 65 (5) (May 2002) 051916.
[37] H. Winkler, A.I. Chumakov, A.X. Trautwein, Nuclear resonant forward and nuclear inelastic scattering using synchrotron radiation for spin crossover systems, in: P. Gütlich, H.A. Goodwin (Eds.), Spin Crossover in Transition Metal Compounds III, in: Topics in Current Chemistry, vol. 235, Springer, 2004, pp. 137–152.

[38] G.J. Long, R.P. Hermann, F. Grandjean, E.E. Alp, W. Sturhahn, C.E. Johnson, D.E. Brown, O. Leupold, R. Rüffer, Strongly decoupled europium and iron vibrational modes in filled skutterudites, Phys. Rev. B 71 (14) (2005) 140302.
[39] S. Tsutsui, J. Umemura, H. Kobayashi, Y. Yoda, H. Onodera, H. Sugawara, D. Kikuchi, H. Sato, C. Sekine, I. Shirotani, ^{149}Sm nuclear resonant inelastic scattering of Sm-based filled-skutterudite compounds, Phys. B: Condensed Matter 383 (2006) 142–143.
[40] Yu.V. Shvyd'ko, M. Lerche, J. Jäschke, M. Lucht, E. Gerdau, M. Gerken, H.D. Rüter, H.-C. Wille, P. Becker, E.E. Alp, W. Sturhahn, J. Sutter, T.S. Toellner, γ-ray wavelength standard for atomic scales, Phys. Rev. Lett. 85 (3) (July 2000) 495–498.
[41] E. Gluskin, E.E. Alp, I. McNulty, W. Sturhahn, J. Sutter, A classical Hanbury Brown–Twiss experiment with hard X-rays, J. Synchrotron Radiation 6 (1999) 1065–1066.
[42] Yu.V. Shvyd'ko, M. Lerche, H.-C. Wille, E. Gerdau, M. Lucht, H.D. Rüter, E.E. Alp, R. Khachatryan, X-ray interferometry with microelectronvolt resolution, Phys. Rev. Lett. 90 (1) (January 2003) 013904.
[43] M. Yabashi, K. Tamasaku, T. Ishikawa, Measurement of X-ray pulse widths by intensity interferometry, Phys. Rev. Lett. 88 (24) (May 2002) 244801.
[44] R. Röhlsberger, K. Schlage, T. Klein, O. Leupold, Accelerating the spontaneous emission of X rays from atoms in a cavity, Phys. Rev. Lett. 95 (9) (2005) 097601.
[45] A. Barla, J.P. Sanchez, Y. Haga, G. Lapertot, B.P. Doyle, O. Leupold, R. Rüffer, M.M. Abd-Elmeguid, R. Lengsdorf, J. Flouquet, Pressure-induced magnetic order in non-magnetic SmS, in: ESRF Highlights 2003, February 2004, pp. 6–7.
[46] L. Pasquini, A. Barla, A.I. Chumakov, O. Leupold, R. Rüffer, A. Deriu, E. Bonetti, Scale effects on the vibrational properties of nanocrystalline iron, in: ESRF Highlights 2002, February 2003, pp. 57–58.
[47] A. Gupta, M. Gupta, S. Chakravarty, R. Rüffer, H.-C. Wille, O. Leupold, Iron self-diffusion in amorphous and nanocrystalline alloys using nuclear resonance reflectivity, in: ESRF Highlights 2005, February 2006, pp. 8–9.
[48] R. Röhlsberger, J. Bansmann, V. Senz, K.-L. Jonas, A. Bettac, O. Leupold, R. Rüffer, E. Burkel, K.-H. Meiwes-Broer, Magnetic order in ultrasmall iron islands on Tungsten(110), in: ESRF Highlights 2001, February 2002, p. 69.
[49] T. Klein, R. Röhlsberger, K. Schlage, H. Thomas, O. Leupold, E. Burkel, Imaging the magnetic structure of exchange-coupled thin films, in: ESRF Highlights 2004, February 2005, pp. 11–12.
[50] A.I. Chumakov, I. Sergueev, U. van Bürck, W. Schirmacher, T. Asthalter, R. Rüffer, O. Leupold, W. Petry, Universal dynamics of glasses, in: ESRF Highlights 2004, February 2005, pp. 7–8.
[51] M. Sekula, S. Pawlus, S. Hensel-Bielowka, J. Ziolo, M. Paluch, C.M. Roland, Structural and secondary relaxations in supercooled di-*n*-butyl phthalate and diisobutyl phthalate at elevated pressure, J. Phys. Chem. B 108 (2004) 4997–5003.
[52] I. Sergueev, U. van Bürck, A.I. Chumakov, T. Asthalter, G.V. Smirnov, H. Franz, R. Rüffer, W. Petry, Rotational and translational dynamics studied by nuclear resonant scattering, in: ESRF Highlights 2003, February 2004, pp. 12–13.